ORIGINAL CONTRIBUTION

Improvement of MR Images Using a Wireless Axial Pair Resonator

Hisatoshi MAEDA[1], Yoko ANDO[1], Nobuo TOYOOKA[2]

[1]*Department of Radiology, Nagoya First Red Cross Hospital*
3-35 Michishita-cho, Nakamura-ku, Nagoya 453
[2]*Department of Radiology, Okazaki Municipal Hospital*

The authors constructed a wireless axial pair resonator (WAPR) to improve the receiver response of the body coil to an incoming signal in a standard 0.5T superconducting magnetic resonance (MR) imaging system. The WAPR consisted of a pair of coils, which were placed in anterior and posterior positions sandwiching a human subject, and was inductively coupled with the body coil.

The enhancement rate of signal intensity (ERSI) was first estimated numerically by using a simple electric circuit model. The signal intensity (SI) and signal-to-noise ratio (SNR) were measured experimentally by imaging the prostate in ten male subjects. The ERSI and SNR enhancement vary as a function of distance between each coil of WAPR, and were approximated by the following equations : ERSI$=2.213-0.046\times$ (intercoil distance in cm), $r=0.803$, and SNR enhancement$=2.284-0.050\times$ (intercoil distance in cm), $r=0.823$. Their average values were 1.23 ± 0.11 and 1.23 ± 0.12 times, respectively.

Improvement of image quality was assessed on T_2-weighted images of the chest, abdomen, and pelvis obtained with and without use of the WAPR. Delineation of the portal and hepatic veins was compared between the two kinds of T_1-weighted images : one taken by using the WAPR with a 20 cm field of view (FOV) and a 224×224 matrix size, and the other taken without using the WAPR with a 35 cm FOV and a 256×192 matrix size. The former image exhibited more veins of small diameter, and showed the veins with greater clarity than the latter image ($p<0.005$). This preliminary imaging indicates that an improvement of image quality is achieved by using the WAPR without having to modify an MR system.

Keywords MR imaging, resonator, receiver coil

INTRODUCTION

MR images have frequently been employed to display the internal structure of various organs because of their excellent contrast resolution for soft tissues and their multiplanar capability features. Commercially available, standard MR systems are generally equipped with large-bore body coils designed to take images of the chest, abdomen, and pelvis. The large-bore body coils have limited ability in reducing acquisition time when ordinary spin-echo sequences are used, and in obtaining high-resolution images when detailed analyses are required[1),2)].

There are several techniques to overcome these limitations, however, including increasing the number of signal averagings by adopting fast acquisition sequences[3)], as well as the use of auxiliary devices[4)~7)].

An inductively coupled coil has been used in MR spectroscopy[8)~11)]. The signal transmission and reception are accomplished with an inductive coupler. The authors made an axial pair resonator[12)] composed of two coils with their axes in line (axial pair), using a body coil as a pickup coil. This type of resonator has a more uniform sensitivity between the two coils and a larger FOV than a single coil of the same diameter. Therefore, this axial pair configuration is suitable for imaging regions deep inside the body.

MATERIALS AND METHODS

The basic scheme of the inductively coupled WAPR is indicated in Fig.1. The following equation[12)] gives an expression for the signal current of the body coil (I_b) as induced by the signal current of the test coil, which is

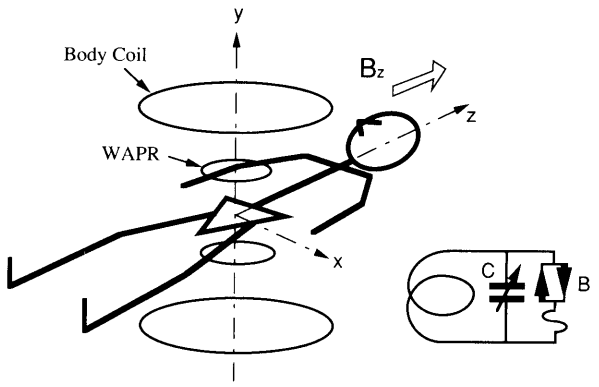

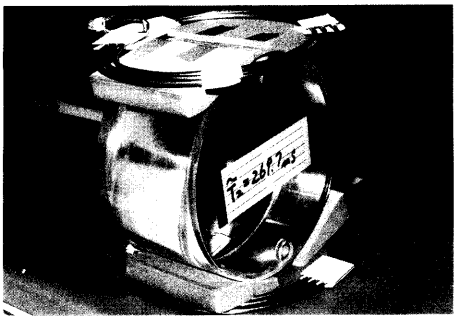

Fig.1. Diagram of wireless axial pair resonator (WAPR).
(a) Each coil of the WAPR is set over and under the lower abdomen of the subject. Inset represents a coil of WAPR : B is a blocking circuit and C is a variable capacitor. The actual body coil is a bird-cage type. (b) A photograph of the WAPR. The loop has three turns of 5mm copper rod ring of 20cm diameter in flat configuration. Each coil of the WAPR consists of a loop, a variable capacitance, and a blocking circuit.

Received Oct. 13, 1993 ; revised Aug. 29, 1994

placed at the center of WAPR coils :

$$I_b = I_o \frac{\sqrt{1+\frac{K_{bw}^2 K_{wt}^2 Q_w^2}{K_{bt}^2}}}{1+K_{bw}^2 Q_b Q_w} \quad (1)$$

I_0 is the current in the body coil without using the WAPR, Q is a quality factor, and K is a coupling constant. The subscripts b, w, and t denote the body coil, the WAPR, and the test coil, respectively.

The ERSI was evaluated using the law of Biot-Savart[13] and the appropriate parameters of Q_b of 240 and Q_w of 80 for various distances between the paired WAPR coils.

The ERSI and SNR enhancements were measured in ten consecutive male patients (average age 66.9±9.8 years) referred for MR studies of bladder cancer. All the patients assumed a supine position with an elastic band placed around the abdomen. An endorectal balloon, inflated with 40ml of air, was placed in the rectum to create an air-filled space as a base for the background. Informed consent was obtained orally from all patients before imaging.

Transaxial images cutting through the prostate and the balloon simultaneously were acquired. The images were acquired twice successively without using the WAPR first, and then images were acquired at the same location with one of the WAPR coils set under the nates and the other coil on the mons pubis.

The following acquisition parameters were used : a single-echo, single-section, 350 ms repetition time[TR]/ 20 ms echo time [TE], FOV 20 cm, matrix size 224×224, section thickness 7 mm, and two-signal averaging. The phase-encoding gradient was set in the anterior to posterior direction. The receiver gain was kept constant during the study. An automated adjusting mode was selected for excitations because the transmission gains were different between these two procedures. It took from 45 to 60 minutes to complete each study.

The signal intensity (SI) was measured on the monitor at the prostate using an operator-defined rectangular region of interest (ROI, 1 cm×1 cm,about 120 pixels). Standard deviations (SD) of the air-filled space at the endorectal balloon were obtained from the difference between the two successive images using a similar ROI. The SI at the prostate and the SD of the air-filled space were measured form five different locations . The SNR was obtatined by dividing the average values of SI by those of SD (NEMA's method [14]). The valuse of ERSI and SNR enhancement for the images taken with and without the WAPR were evaluated, and these valuse were plotted against various intercoil distances.

Images were obtained with and without the WAPR employing the identical acquisition parameters : a single-echo, multi-section, TR/TE 2,000/100, FOV 20 cm, matrix size 224×224, section thickness 7 mm, slice interval 1 mm, and two-signal averaging. Images of the chest, abdomen, and pelvis were acquired from three patients.

Two different kinds of hepatic images, one with an FOV 20 cm and the other with an FOV 35 cm, were obtained from eight patients referred for MR studies of hepatic tumors. FOV 20 cm images were obtained from July to August 1992 from three patients (two men and one woman with an average age of 57.0 years). FOV 35 cm images were obtained from January to March 1992 from

five patients (three men and two women with an average age of 53.6 years). FOV 20 cm T_1-weighted axial images were acquired with the following acquisition parameters : multi-section, single-echo, TR/TE 390-450/16-20, matrix size 224×224, section thickness 7 mm, slice interval 1 mm, four-signal averaging, and with respiratory compensation. FOV 35 cm images were acquired with these parameters : multi-section, single-echo, TR/TE 650-700 /16, matrix size 256×192, section thickness 7 mm, slice interval 1 mm, four-signal averaging, and with respiratory compensation.

A section one or two slices above the hilar region on the image film was seleted . All the portal and hepatic veins which were identified on the visual inspection, and which ran parallel to the section plane, were marked. The diameters of the vein (D) were measured on the image film and the veins were divided into three groups : 1) D less than or equal to 2 mm, 2) D greater than 2 mm and less than or equal to 5 mm, and 3) D greater than 5 mm. Two radiologist and four residents grouped each vein marked into three categories of visualization : good, fair, and poor. The numbers of the count for each category were plotted against different groups of D. The statisical analyses were performed by using the Mann-Whitney rank-sum test and contingency table.

All images were obtained with a commercial 0.5-T system (RESONA, Yokogawa Medical Systems Co., Tokyo) without any modification.

RESULTS

The predicted values of ERSI for various intercoil distances are listed in Table 1. Measured valuse of ERSI and SNR enhancements in the human subjects are plotted in Fig.2a. Figure 2b indicates the image of the prostate and the endorectal balloon taken during the measurements of ERSI and SNR. The average ERSI and SNR enhancements were 1.23±0.11 and 1.23±0.12, respectively, with an average intercoil distance of 21.1±2.0 cm. The regression lines were : ERSI Improvement=2.213−0.046×(Intercoil distance in cm), r=0.803 (n=10), and SNR enhancement = 2.284−0.050×(Intercoil distance in cm), r=0.823 (n=10).

Figures 3 through 5 are the T_2-weighted images of the chest, abdomen, and pelvis. The tumor margins and the inner structures are more clearly delineated on the images A taken with the WAPR than the images B taken without the WAPR.

There were 31 veins on three FOV 20 cm images and 36 veins on five FOV 35 cm images. Typical T_1-weighted hepatic images are shown in Fig.6. The smallest diameters of the veins discriminated on these images were 0.9 mm and 1.4 mm. The average diameters

Table 1. Calculated Values of Enhancement Rate of Signal Intensity (ERSI)

ICD	K_{bw}	K_{wt} / K_{bt}	ERSI
15.0	1.69 10^{-2}	11.29	2.36
17.5	1.81 10^{-2}	9.40	1.87
20.0	1.94 10^{-2}	7.80	1.47
22.5	2.08 10^{-2}	6.47	1.16
25.0	2.23 10^{-2}	5.37	0.92

ICD is the intercoil distance of the WAPR paired coils (in centimeters). K and SI denote coupling constant and signal intensity. Subscripts b, w, and t stand for body coil, WAPR, and test coil, respectively. Values of ERSI were calculated from Eq. (1) in the text.

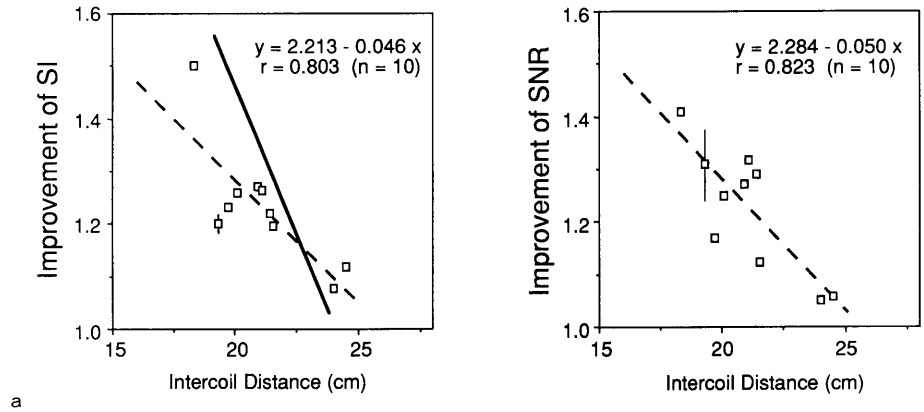

Fig.2. Enhancement rate of signal intnesity (ERSI) and signal-to-noise ratio (SNR) improvement for different values of intercoil distances of WAPR. (a) Squares depict the observed values of ERSI and SNR enhancement, respectively. Typical error bars are shown. Broken lines denote the regression lines of the observed ERSI and enhancement. Solid line represents the values of ERSI computed from Eq. (1). (b) Typical images of the prostate (arrow) and endorectal balloon (*) taken during the measurements of ERSI and SNR enhancement. A is obtained by using the WAPR and B is obtained without using the WAPR.

were 2.44±1.65 mm, and 3.47±1.75 mm on the FOV 20 cm and FOV 35 cm images, respectively ($P<0.004$, Mann-Whitney rank-sum test). Frequencies in each category of visualization are plotted in Fig.7 against a different group of D on the FOV 20 cm images and on the FOV 35 cm images. Seventy-three percent of the vessels with $D\leqq2$ mm and 96% of the vessels with $2<D\leqq5$ mm were scored good to fair on the FOV 20 cm images, whereas 50% of the vessels with $D\leqq$ 2 mm and 93% of the vessels with $2<D\leqq5$ mm were scored good to fair on the FOV 35 cm images. In comparison with the FOV 35 cm images, the FOV 20 cm images exhibited significantly clearer images of the veins with a D less than or equal to 5 mm (for $D\leqq2$ mm, $p<0.005$, and for 2 mm$<D\leqq5$ m, $p<0.004$, contingency table). There was no statistical difference between these images in the delineation of the veins with $D>5$ mm.

DISCUSSION

Equation (1) is approximately proportional to K_{wt}/K_{bw} for the values of coupling constant listed in Table 1. The K_{bw} (coupling constant between the body coil and WAPR) increases and the K_{wt} (coupling constant

A B

Fig.3. A squamous cell carcinoma of the right superior pulmonary sulcus (Pancoast's tumor) in a 53-year-old man. The subject suffered from pain in the right shoulder and numbness of the right hand. Image A is taken without the WAPR and B is taken using the WAPR. Extrapleural invasion of the tumor (arrow) is more clearly depicted in B than in A.

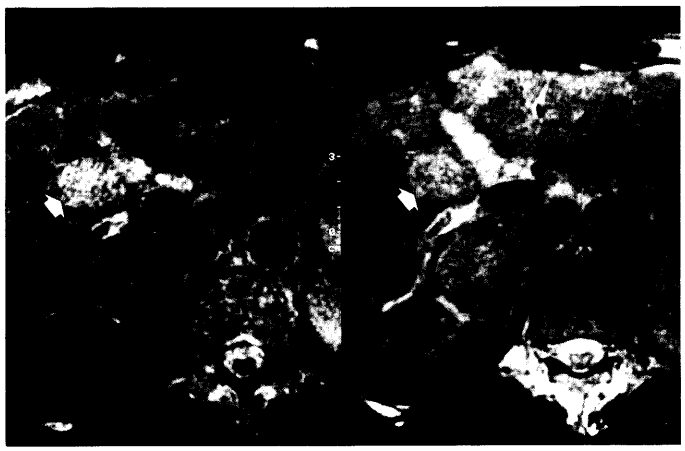

A B

Fig.4. Metastatic liver tumor in a 63-year-old man. A mass (arrow) is depicted in the antero-superior segment of the right lobe. Image A is grainier than image B.

between the WAPR coil and test coil) decreases, when the distance between the WAPR and test coil increases. Therefore, the ERSI decreases as the intercoil distance of WAPR increases.

The resonant frequency as well as the quality factor Q_w of WAPR vary among the subjects and with the intercoil distance. A frequency shift of 3% and a reduction of Q_w of 50% from the unloaded state ensued when the WAPR was loaded with a particular subject (H. M., 172 cm, 64 Kg). These values are much greater than the actual variation in frequency shift and Q_w among the different subjects. The observed ERSI (Fig.2a) had diffrernt values from those predicted from

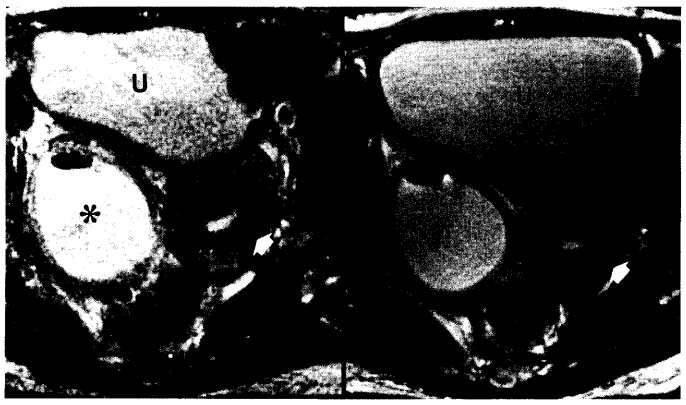

Fig.5. Escherichia coli abscess of the right ovary in a 41-year-old patient with diabetes mellitus. Fluid of high signal intensity (*) encapsulated in a shell of uniform thickness is shown dorsal to the urinary bladder (U) and to the right of the uterus (arrow). The air-fluid level of the abscess is more clearly shown in B, taken using the WAPR, than in A, which was taken without the use of the WAPR.

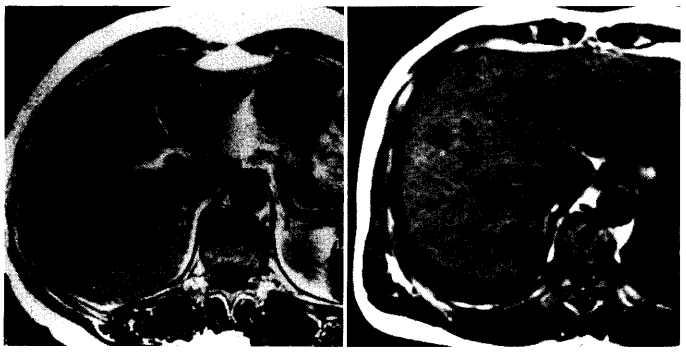

Fig.6. An FOV 20 cm image (A) and an FOV 35 cm image (B). A and B are from a 62-year-old woman and a 40-year-old man, respectively.

Eq. (1), with the largest difference of 40%. A resonant-frequency shift of 0.5% (100kHz) resulted in 40% ERSI change for the system with Q valuse of 80. The constitutions of the subjects, especially the lipid content of the body, influenced the resonant-frequency. Individual resonant-frequency adjustment could have improved ERSI further, but this was thought to be impractical and unnecessary, and no resonant-frequency adjustment for subjects was made.

When the intercoil distance was less than 17 cm, the SNR enhancement became greater than the square root of 2 (Fig.2). The same SNR as achieved without using the WAPR could be achieved with half the number of signals averaging. On the other hand, when the intercoil distance is greater than 26 cm, the SNR enhancements are less than unity, as indicated by the regression line in Fig.2a. Applications of the WAPR should be chosen carefully because no benefit is reaped in some

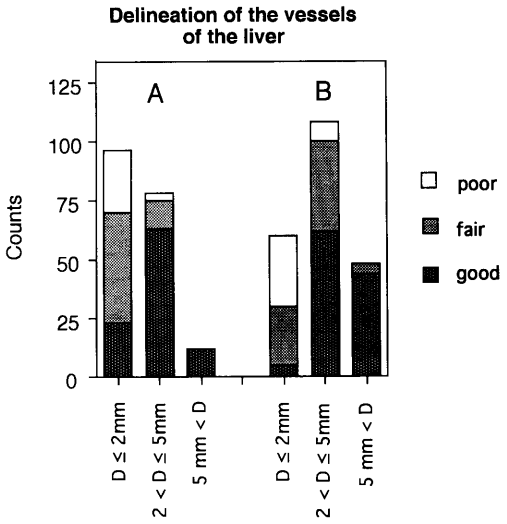

Fig.7. Delineation of the vessels of the liver. Image quality of the portal and hepatic veins is grouped as good, fair, or poor for various diameter (D) of the veins. A and B are for the FOV 20cm image and for the FOV 35cm image, respectively. Refer to the text for details.

cases.

The experimental SNR did not vary in parallel with the ERSI (Fig.2a). Because the noise present in the coil is a function of coil resistance[15], the SNR is proportional to the current in the body coil, and is thus proportional to the signal intensity. The noise generated in the object is due to dielectric loss, and the Bl field generated by the axial pair coils disturbs the main magnetic field. The pulsatile blood flow as well as the respiratory motion of the abdominal wall cause the SNR to decrease. These phenomena cause the observed discrepancies between ERSI and SNR.

The average diameter of the veins identified on the FOV 20 cm images is smaller than those on the FOV 35 cm images. The respective pixel sizes of FOV 20 cm and FOV 35 cm images are 0.9 mm×0.9 mm and 1.4 mm×1.8 mm. Images of smaller pixel size are expected to exhibit veins with smaller diameter.

The FOV 20 cm image theoretically has an SNR 0.75 time lower than the FOV 35 cm image under the assumptions that a 1.23 ERSI is realized by using the WAPR, and that the same TR/TE values is employed. The FOV 20 cm image in Fig.6A is thus apparently more grainy than the image in Fig.6B. However, Fig.7 indicates that the veins are more clearly delineated on the FOV 20 cm image. The probable reasons why the FOV 20 cm image affords clearer images of the veins than the FOV 35 cm image does are: 1) we adopted a shorter TR in acquiring the FOV 20 cm images, which introduced a greater tissue contrast between the vessels and the surrounding liver tissue ; 2) the FOV 20 cm image requires a larger number of pixels to cover an area than the FOV 35 cm image, leading to an impression of clearer margins for the veins ; and 3) the motion artifact was less obvious on the short TR and TE images.

Because the WAPR is equipped with a blocking circuit and the coils are isolated electrically with insulators, the WAPR can be applied safely without posing any high-voltage hazards to patients or MR systems.

The use of the WAPR is easy : the only requirement for adopting the WAPR involves setting the target area between the two coils without preparation of patients. The WAPR is neither particularly difficult nor expensive to fabricate, and the use of the WAPR ensures no change in the front-end electronics of the system. The authors cannot conceive of any objection to the use of the WAPR in

ordinary MR studies, although improvement in the SI and SNR is marginal.

ACKNOWLEDGMENTS

The authors would like to express their thanks to Dr. H. Watari and Mr. H. Okawara of the National Institute of Physiological Sciences for their advice and help in the preparation of resonators, to Dr. T. Ishigaki at Nagoya University for discussions on the use of the WAPR, and to Dr. A. Nagano, Dr. T. Okada, Dr. N. Mutsuga, and Dr. K. Watanabe at Nagoya First Red Cross Hospital for their help in evaluation of image quality of hepatic vessels.

REFERENCES

1) Dooms GC, Hricak H : Magnetic resonance imaging of the pelvis ; prostate and urinary bladder. Urol Radiol, 8 : 156-165, 1986.
2) Carrol CL, Sommer FG, McNeal JE, Stamey TA : The abnormal prostate ; MR imaging at 1.5T with histopathologic correlation. Radiology, 163 : 521-525, 1987.
3) Mitchell DG : Abdominal magnetic resonance imaging : optimization and artifact suppression. Top Magn Reson Imaging, 4 : 18-34. 1992.
4) Barentsz JO, Lemmens JAM, Ruijs SHJ, et al. : Carcinoma of the urinary bladder : MR imaging with a double surface coil. AJR, 151 : 107-112, 1988.
5) Smith RC, Reinhold C, McCauley TR, et al. : Multicoil high-resolution fast spin-echo MR imaging of the female pelvis, Radiology, 184 : 671-675, 1992.
6) Schnall MD, Lenkinski RE, Pollack HM, Imai Y, Kressel HY : Prostate : MR imaging with an endorectal surface coil. Radiology, 172 : 570-574, 1987.
7) Milestone BN, Schnall MD, Lenkinski RE, Kressel HY : Cervical carcinoma ; MR imaging with an endorectal surface coil. Radiology, 180 : 91-95, 1991.
8) Chen CN, Holt DI, Sank VJ : Quadrature detection coils-a further square root of 2 improvement in sensitivity, J Magn Reson, 54 : 324-327, 1983.
9) Hoult DI, Chen CN, Sank VJ : Quadrature detection in the laboratory frame. J Magn Reson, 1 : 339-353, 1984.
10) Schnall MD, Barlow C, Subramanian JS, Leigh JS Jr : Wireless implanted magnetic resonance probes *in vivo* NMR. J Magn. Reson, 68 : 161-167, 1986.
11) Decorps M, Blondet P, Reutenauer H, Albrand JP, Remy C : An inductively coupled, series-tuned NMR probe. J Magn Reson, 65 : 100-109, 1985.
12) Maeda H, Toyooka N, Okawara H : A wireless axial pair resonator. Magn Reson Med, 29 : 567-570, 1993.
13) Purcell EM : A universal law of induction ; Electricity and magnetism. Berkeley Physics Course, McGraw-Hill, New York, 1965. pp240-250.
14) National Electrical Manufacturer Association MS-1 : Determination of signal-to-noise ratio (SNR) in diagnostic magnetic resonance images. NEMA, washington, D. C. 1988.
15) Hoult DI, Richards RE : The signal-to-noise ratio of the nuclear magnetic resonance experiment. J Magn Reson, 24 : 71-85, 1976.